MODELLING AND FABRICATION OF A MECHANICAL CELL STIMULATOR

Yongjun Lai[1], Evgueni Bordatchev[2]
[1] Department of Mechanical and Materials Engineering
Queen's University
Kingston, ON, K7L 3N6
[2] Integrated Manufacturing Technologies Institute
National Research Council of Canada
800 Circle Collip, London, Ontario, Canada, N6G 4X8
Contact: lai@me.queensu.ca

Received June 2007, Accepted November 2007
No. 07-CSME-54, E.I.C. Accession 3023

ABSTRACT

In the field of tissue engineering, mechanical cell stimulators are widely used to simulate forces in natural body environments, or to accelerate the growth of tissue. Simulation of the natural body environment, *in vitro*, enables researchers to understand the effect of different disturbance on cells, independently. For tissue such as the cartilage, which grows relatively slow in a mature natural body environment, a cell stimulator can be used to speed up the growth of tissue. This paper presents a novel design of planar mechanical cell stimulator which is able to provide mobility of four. The stimulator was fabricated from polymethyl-methacrylate (PMMA) thin plates using advanced micromilling material-removal process with an accuracy of ±3 μm and a surface roughness of 120 nm. The kinematic model of the stimulator is developed and corresponding performance is simulated.

MODELAGE ET FABRICATION D'UN STIMULATEUR MECANIQUE DE CELLULES

RESUME

Dans le domaine de l'ingénierie tissulaire, les stimulateurs mécaniques de cellules sont couramment employés pour simuler les forces ayant cours dans le milieu naturel du corps ou pour accélérer la croissance des tissus. Cette simulation *in vitro* du milieu naturel du corps permet aux chercheurs de mieux comprendre l'effet de diverses perturbations sur les cellules de façon indépendantes. Pour des tissus tel que le cartilage, dont le développement en milieu mature est relativement lent, l'utilisation d'un stimulateur cellulaire peut être employé pour accélérer leurs croissances. Cet article présente une conception novatrice d'un stimulateur mécanique de cellules permettant de fournir une mobilité avec quatre degrés de liberté. Le stimulateur a été fabriqué à partir de plaques minces de polyméthyle-méthacrylate (PMMA) en utilisant un procédé avancé de micro-usinage avec une précision de ±3 μm et une rugosité de surface de l'ordre de 120 nm. Le modèle cinématique du stimulateur est développé et la performance correspondante du modèle est simulée.

INTRODUCTION

Although tissue engineering of articular cartilage is a promising approach for cartilage repair, it has been difficult to develop cartilaginous tissue in vitro that mimics the properties of native cartilage. Isolated hondrocytes grown in culture typically do not accumulate enough extracellular matrix, and the generated tissue possesses only a fraction of the mechanical properties of native cartilage. One potential explanation for this might be that the cells are grown in an environment that lacks the mechanical stimuli to which the chondrocytes are exposed in vivo [1, 2], and corresponding investigations regarding mechanical stimuli of cell have been conducted extensively.

The state-of-the-art mechanical cell stimulators have several popular types: hydrostatic pressurization, longitudinal stretching, substrate bending, fluid shearing, etc. Hydrostatic pressurization [3, 4], including negative (vacuum) or positive pressurization [5], compressive loading system [6], use a moving plate to compress the tissue on contact (Fig. 1a), and later use direct platen abutment [7 -9] (Fig. 1b). However, in vivo stress states that tissue experiences depart very substantially from purely hydrostatic pressure and in experiments. The parameters of the mechanical stimulus itself have not usually been quantified [10]. Longitudinal stretch systems [11 -14] utilize controlled uniaxial distention of deformable substrates on which cell sheets grow to deliver the mechanical stimuli (Fig. 1c). Due to the Poisson effect, grip end effect and geometric irregularity of substrate, etc., such systems inevitably introduce undesired heterogeneous local strains. Substrate bending systems [15–16] use substrate flexure to provide an alternative means for delivering longitudinal strains to a culture surface (Fig. 1d). Fluid shear systems apply fluid shear stress to cell culture using two popular approaches: cone and plate flow chamber (Fig. 1e) and parallel plate flow chamber (Fig. 1f). The shear stresses are controlled by angular velocity and pressure gradient, respectively.

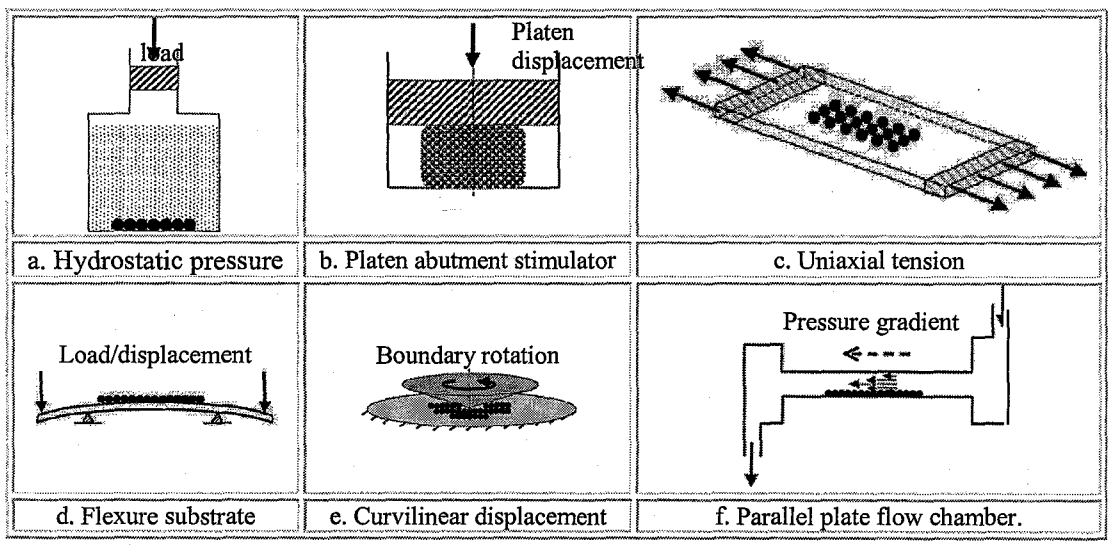

Figure 1. Schematic diagrams of several state-of-the-art mechanical stimulators [10].

Most state of the art stimulators are limited to providing uniaxial tension, compression, or 2D in plane stretching for a monolayer. The stimuli from such stimulators are too simple compared to the actual complexity of the cell grow environment in human body. The proposed cell stimulator with at least 4 Degrees-of-Freedom (DOF) is able to provide versatile stimuli (the stimulator has four stimulating pads and each pad has 1DOF).

Flexible substrates, working as compliant mechanisms, are widely used in the existing cell stimulation. Compared to rigid-body mechanisms, compliant mechanisms require considerably less number of components. The reduction in part numbers leads to simple manufacturing and reduced manufacturing and assembly time and cost. Furthermore, compliant mechanisms also have a smaller number of movable joints (surface contact joints), such as pin and sliding joints. This results in reduced wear and need for lubrication. Compliant mechanisms are either free of assembly, or able to reduce the total number of parts and joints, which is a significant advantage in the micro-fabrication [17-22].

DESIGN OF THE COMPLIANT STIMULATOR

The proposed stimulator is a compliant mechanism consisting of eight rigid links, labeled from 1 to 8 (see Fig. 2), forming a symmetrical loop. There are eight flexible joints connecting two adjacent loop links. Four rigid links (link 9 – link 12) are attached to four of the joints from outside of the loop, and used as driving links. Inside of the loop, there are also four rigid links (link 13 – link 16) attached to another four flexible joints and used as driven links with stimulating pads which will be coated with a biological layer to sustain cells. At this particular stage, the motions of the pads are desired to be linear only. When two facing pads are paired up, they can generate compressive or tensile stimuli of a certain pattern. The flexible joints are formed by removal of material in the conjunction areas, which introduces notches resulting in reduced stiffness. Figures 2b and c show the close-up of the joints with different notch layouts.

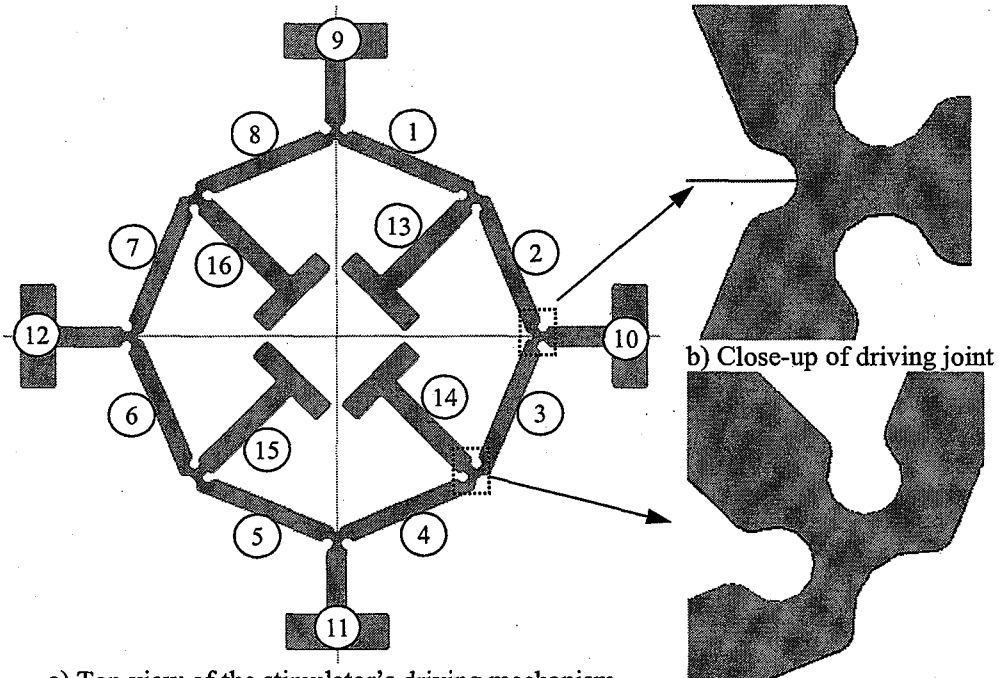

a) Top view of the stimulator's driving mechanism

b) Close-up of driving joint

c) Close-up of driven joint

Figure 2. The 2D layout of the stimulator's driving mechanism.

A guide shell is developed in order to constrain the motion of the stimulating pads. The 2D layout of the guiding shell is illustrated (see Fig. 3a). There are four pieces of structural walls separated by four

trenches/gaps of the same width as the driven links with tolerance of 50μm. The shell walls are located inside the loop and the four stimulating links fit into the four gaps of the walls forming four sliding joints. The central cube in the guiding shell (see Fig. 3b) is to fit into the central cube space of the stimulator (see Fig. 3c) during the biological coating process. After that, the central cube will be removed, and a cell unit will fill the empty central space and attach to the surfaces of the stimulating pads.

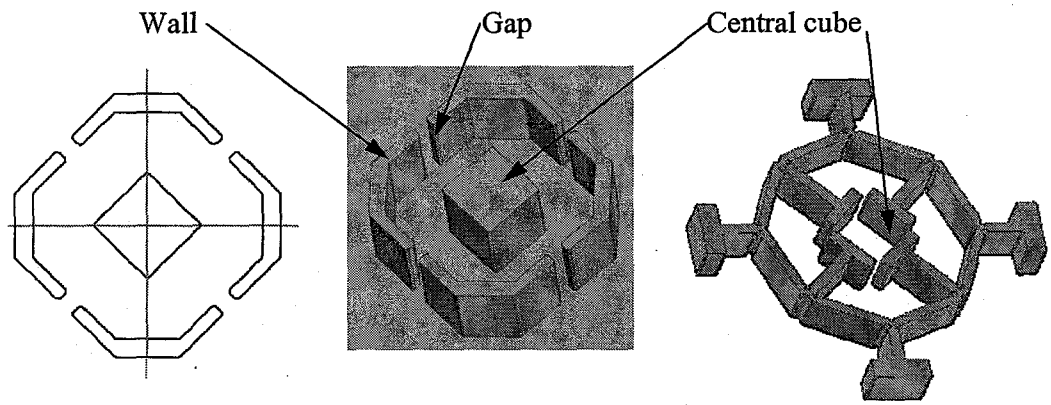

a) Top view of guiding shell b) 3D view of guiding shell c) 3D view of stimulator

Figure 3. The layout of the stimulating mechanism and its guiding shell.

FABRICATION

The micromilling material-removal process is a scaled-down analog of the conventional milling machining process using direct drive spindles with a high rotational speed of up to 200,000 rpm, high travel speed of up to 500 mm/s, and small micromills with a diameter of as small as 25 μm. The scaling-down effect brings significant advantages of the conventional milling process into high-precision microfabrication with respect to other micromachining technologies, e.g. laser micromachining. However, it also introduces new challenges associated with tool handling, alignment, chip removal, process-parameter optimization and process planning. The stimulator was fabricated from polymethyl-methacrylate (PMMA) thin plates with a thickness of 3mm and 1 mm using the micromill with a diameter of 350 μm. Use of high-precision motion stages with positional accuracy of 0.5 μm in a combination with a high cutting speed of 4 m/s allowed fabrication of the functional stimulator prototype with an accuracy of ±3 μm and a machined average surface roughness of 120 nm as shown in Figure 4. Figure 5a illustrates a prototype of the stimulating mechanism and Fig. 5b shows the assembly of the stimulating mechanism and its guiding shell.

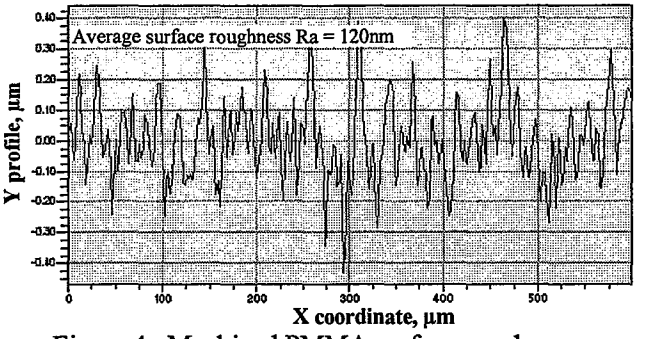

Figure 4. Machined PMMA surface roughness.

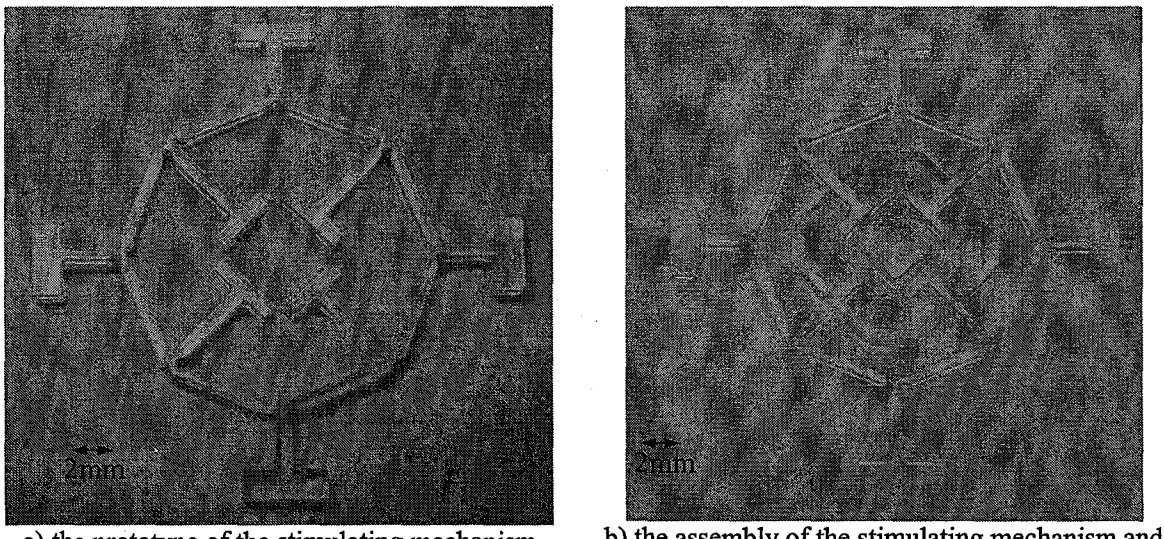

a) the prototype of the stimulating mechanism

b) the assembly of the stimulating mechanism and its guiding shell

Figure 5. Photograph of the prototype

KINEMATIC MODELLING AND SIMULATION

The structure has a uniform thickness of 1 mm, which is 2 times the width of the rigid links. Therefore, the out-of-plane stiffness of the structure is relatively higher than the one in-plane. The driving force is in-plane; consequently, the structure kinematic model is reasonably treated as a planar mechanism. Since the flexible joints, formed with notches, allow relative rotations much easier than other motions, the flexible joints are modeled as rotary joints. The stimulating links are guided by the guiding wall and can only translate along one direction; therefore, sliding joints are used as their kinematic constraints. The kinematic model is in Fig. 6. The mechanism has 17 links (including a frame), and it has eight doubled rotary joints and four sliding joints. According to the Gruebler's equation [23], the mobility of the mechanism can be calculated:

$$m = 3(n-1) - 2l \tag{1}$$

where n is the number of the links, and l is the number of lower pairs. Substituting n = 17 and l = 20 into equation (1), the mobility of the mechanism is calculated as 8. Obviously, each of the four driving links (link9-link12) has a local mobility which allows it to rotate around the corresponding rotary joint. There are four actuators that are used to drive the stimulating mechanism described briefly elsewhere [18]. The actuators provide only translational motions to the driving links. Figure 6 illustrates an arbitrary configuration of the stimulator by solid lines, and original position of the stimulator by dashed lines.

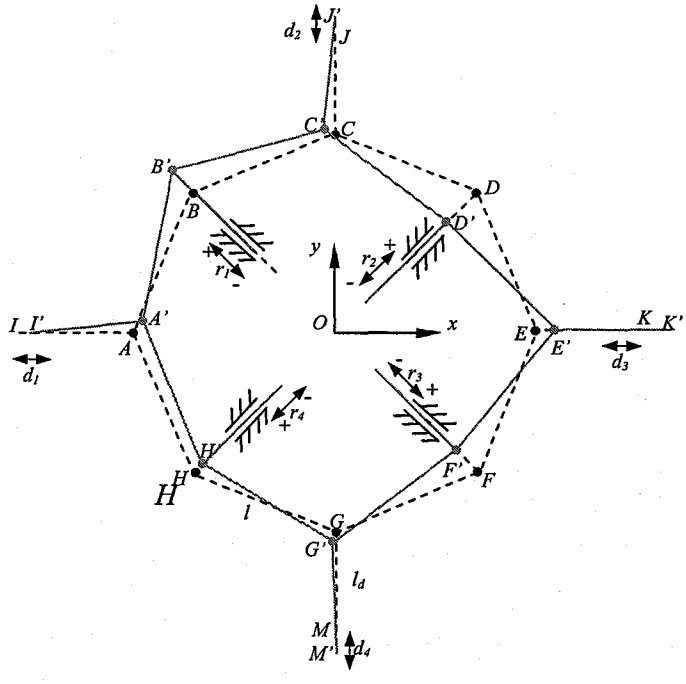

Figure 6. Kinematic model of the stimulator.

The coordinate system is established as shown in Fig. 6. The origin O of the coordinate system is the original centre of the stimulator. The symbols A-H represent the eight rotary joints on the stimulator, and I, J, K, M represent the four joints connecting driving links and corresponding actuators. Due to the restriction of the actuators, I & K can only move in the x direction (horizontal), and J & M can only move in the y direction (vertical). The length of the links (1 to 8) is identical, and denoted by l. The original distance from the origin O to the center of the rotary joints A-H, is denoted by r_0 ($= l \cdot \sin 67.5^o / \sin 45^o$ from the geometry); the output displacements of the stimulating pads are r_i (i =1 to 4). The pads provide either compression or extension to the tissue cube. According to common designation rules of mechanics, compressive stress is negative and tensile stress is positive, therefore, the output displacement is negative when the pad compress the tissue cube, otherwise, it is positive; the input displacement of the actuators are denoted by d_i, (i = 1, to 4). Due to the symmetric geometry of the device, an input displacement can be identified by the geometry of two adjacent output displacements. Therefore, one quarter of the device is sufficient to find out the kinematic relations between input and output displacements. In Fig. 6, HH' ($=r_4$) and FF' ($=r_3$) represent the output motions of the stimulating pads 4 and 3 respectively, where MM' ($=d_4$) is the input displacement of actuator 4. O, H, G, F, and M are the original positions of the joints and

$|\overline{OG}| = |\overline{OH}| = |\overline{OF}| = r_0$, $|\overline{GH}| = |\overline{GF}| = l$, $|\overline{GM}| = l_d$. The new positions of the joints are O', H', G', F', and M'. Theoretically speaking, there will be two solutions for the inverse kinematic relation between input and output displacement (see Fig. 7). However, for this case, the driving motion d_4 is relatively small and the sum of the angles $\angle H'G'M' + \angle F'G'M'$ is always expected to be greater than π due to the physical constraint of the compliant joint. Therefore, the 1st solution is the desired solution for this stimulator. The following process of deriving the inverse kinematic relation between input and output relation will be focused on the 1st solution.

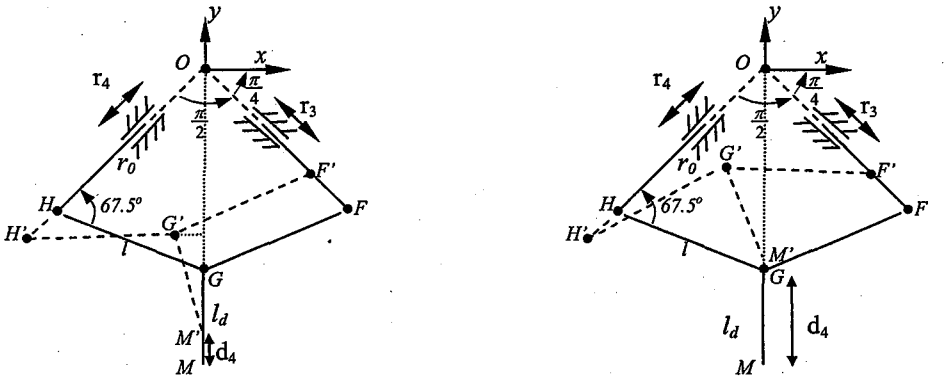

(a) The 1st inverse kinematic solution, (b) the 2nd inverse kinematic solution

Figure 7. The geometry of one quarter of the mechanism under an input displacement.

The input displacement d_4 can be represented by $\overrightarrow{MM'}$, which is equal to $y_{M'} - y_M$. The coordinate of M is:

$$x_M = 0, \tag{2}$$

$$y_M = -|\overline{OG}| - |\overline{GM}| = -r_0 - l_d. \tag{3}$$

The coordinate of M' can be represented by the coordinates of G':

$$x_{M'} = 0 \tag{4}$$

$$y_{M'} = y_{G'} - \sqrt{|\overline{G'M'}|^2 - x_{G'}^2} = y_{G'} - \sqrt{l_d^2 - x_{G'}^2} \tag{5}$$

The coordinate of the G' are found as follows:

$$y_{G'} = (r_0 + r_4)\sin\left(\frac{5\pi}{4}\right) + l\sin\left(\frac{\pi}{4} - \arctan\left(\frac{r_0 + r_3}{r_0 + r_4}\right) - \arccos\left(\frac{\sqrt{(r_0 + r_3)^2 + (r_0 + r_4)^2}}{2l}\right)\right) \tag{6}$$

$$x_{G'} = (r_0 + r_4)\cos\left(\frac{5\pi}{4}\right) + l\cos\left(\frac{\pi}{4} - \arctan\left(\frac{r_0 + r_3}{r_0 + r_4}\right) - \arccos\left(\frac{\sqrt{(r_0 + r_3)^2 + (r_0 + r_4)^2}}{2l}\right)\right) \tag{7}$$

The inverse kinematic relationship can be written as follows:

$$d_4 = y_{M'} - y_M = y_{G'} + r_0 + l_d - \sqrt{l_d^2 - x_{G'}^2} \tag{8}$$

Similarly, the inverse kinematic relation between other input and output displacements are determined as follows:

$$d_2 = y_{C'} - r_0 - l_d + \sqrt{l_d^2 - x_{C'}^2} \tag{9}$$

$$y_{C'} = (r_0 + r_1)\sin\left(\frac{3\pi}{4}\right) + l\sin\left(\arctan\left(\frac{r_0 + r_2}{r_0 + r_1}\right) + \arccos\left(\frac{\sqrt{(r_0 + r_2)^2 + (r_0 + r_1)^2}}{2l}\right) - \frac{\pi}{4}\right) \tag{10}$$

$$x_{C'} = (r_0 + r_1)\cos\left(\frac{3\pi}{4}\right) + l\cos\left(\arctan\left(\frac{r_0 + r_2}{r_0 + r_1}\right) + \arccos\left(\frac{\sqrt{(r_0 + r_2)^2 + (r_0 + r_1)^2}}{2l}\right) - \frac{\pi}{4}\right) \tag{11}$$

$$d_1 = x_{A'} + r_0 + l_d - \sqrt{l_d^2 - y_{A'}^2} \tag{12}$$

$$y_{A'} = (r_0 + r_4)\sin\left(\frac{5\pi}{4}\right) + l\sin\left(\arctan\left(\frac{r_0 + r_1}{r_0 + r_4}\right) + \arccos\left(\frac{\sqrt{(r_0 + r_4)^2 + (r_0 + r_1)^2}}{2l}\right) + \frac{\pi}{4}\right) \tag{13}$$

$$x_{A'} = (r_0 + r_4)\cos\left(\frac{5\pi}{4}\right) + l\cos\left(\arctan\left(\frac{r_0 + r_1}{r_0 + r_4}\right) + \arccos\left(\frac{\sqrt{(r_0 + r_4)^2 + (r_0 + r_1)^2}}{2l}\right) + \frac{\pi}{4}\right) \tag{14}$$

$$d_3 = x_{E'} - r_0 - l_d + \sqrt{l_d^2 - y_{E'}^2} \tag{15}$$

$$y_{E'} = (r_0 + r_2)\sin\left(\frac{\pi}{4}\right) + l\sin\left(\arctan\left(\frac{r_0 + r_3}{r_0 + r_2}\right) + \arccos\left(\frac{\sqrt{(r_0 + r_3)^2 + (r_0 + r_2)^2}}{2l}\right) + \frac{5\pi}{4}\right) \tag{16}$$

$$x_{E'} = (r_0 + r_2)\cos\left(\frac{\pi}{4}\right) + l\cos\left(\arctan\left(\frac{r_0 + r_3}{r_0 + r_2}\right) + \arccos\left(\frac{\sqrt{(r_0 + r_3)^2 + (r_0 + r_2)^2}}{2l}\right) + \frac{5\pi}{4}\right) \tag{17}$$

According to the inverse kinematic relation of input and output displacements identified as above, the required displacements from the actuators in order to generate a specific pattern of stimuli can be predicted. Figure 8 illustrates simulated three patterns of stimuli and corresponding actuations that required to generate such stimuli using l = 6 mm, l_d = 3 mm.

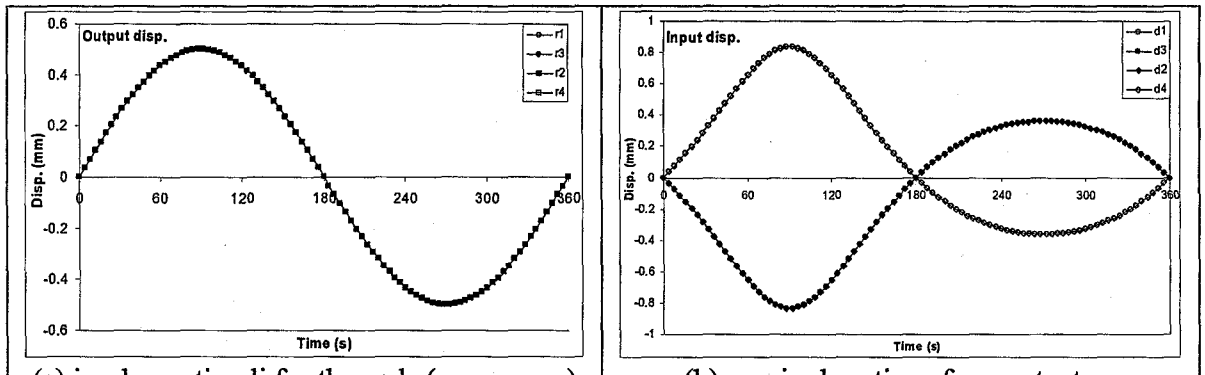

(a) in-phase stimuli for the pads (r_1=r_2=r_3=r_4) (b) required motions from actuators

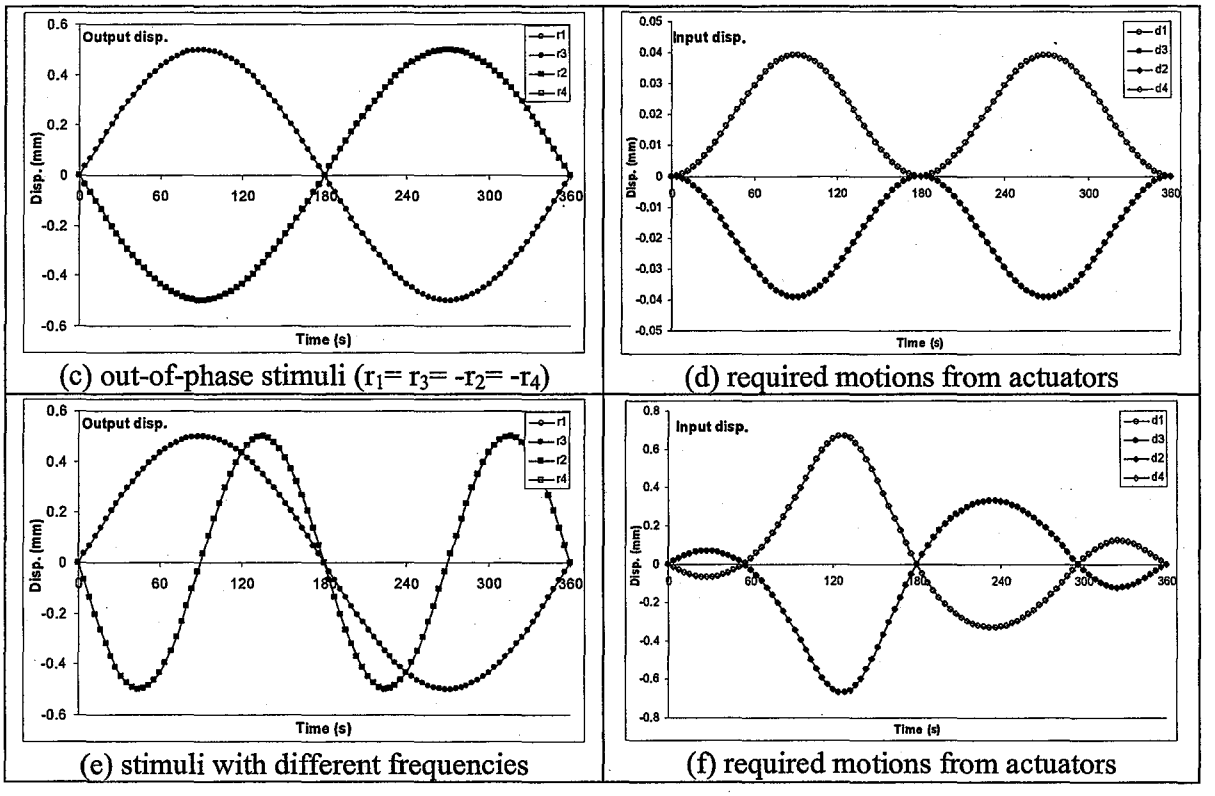

(c) out-of-phase stimuli ($r_1 = r_3 = -r_2 = -r_4$) (d) required motions from actuators

(e) stimuli with different frequencies (f) required motions from actuators

Fig. 8. Simulation of stimuli of given specific patterns and required actuator motions.

Figure 8*a* is the stimuli of the four pads (r_1 and r_3, r_2 and r_4) move in-phase and with the same magnitude. The actuations that required generating such stimuli are given in Fig. 8b. Figures 8a and b say that the driving actuators should follow: $d_1 = - d_3$, and $d_2 = - d_4$. The magnitudes of the input and output displacements are at the similar level. Figures 8c and 8d show that when the pads provide out-of-phase stimuli, the input displacements have been amplified approximately 10 times by the mechanism. When the pads stimulate cells with different frequencies, the required actuations are more complicated. For instance, Fig. 8e demonstrates the stimuli with different frequencies (frequency of r_2 and r_4 is twice as the frequency of r_1 and r_3), and Fig. 8f shows the required actuations of d_1 to d_4.

CONCLUSIONS

In this paper, a novel cell stimulator was designed, and fabricated using high precision micromilling technology. A kinematic model was developed for the stimulator with mobility of eight, including four local ones. The inverse kinematic solution for the stimulator based on the model developed was obtained, and example was provided to demonstrate the relationship of the desired stimuli and required actuation from the four actuators. Based on this work, in the future dynamic performance and control strategies will be investigated.

ACKNOWLEDGMENTS

This paper is the result of collaboration between Queen's University, Kingston, Ontario, Canada and NRC-IMTI, London, Ontario, Canada. The authors thank Mahmud-Ul Islam, Director, Production Technology Research, NRC-IMTI, and Suwas Nikumb, Group Leader, Precision Fabrication Processes, NRC-IMTI, for their continued support in this work. This study was partially supported by NSERC Discovery Grant R3440A01 and by NRC (Canada)—NSC (Taiwan) Collaborative Research Program.

REFERENCES

[1] Waldman SD, Spiteri CG, Grynpas MD, Pilliar RM, Kandel RA. Long-term intermittent compressive stimulation improves the composition and mechanical properties of tissue-engineered cartilage. *Tissue Eng* 2004, **10(9-10)**: 1323-1331.

[2] Waldman, SD, Spiteri CG, Grynaps MD, Pilliar RM, Hong J and Kandel RA, Effect of Biomechanical Conditioning on Cartilaginous Tissue Formation in Vitro, *Journal of Bone and joint surgery,* 2003, **85A** , Supplement 2, 101-105.

[3] Parkkinen, J.J., Lammi, M.J., Inkinen, R., Jortikka, M., Tammi, M., Virtanen, I., Helminen, H.J., 1995. Influence of short-term hydrostatic pressure on organization of stress "bers in cultured chondrocytes. *Journal of Orthopaedic Research* **13**, 495-502.

[4] Brighton, C.T., Fisher, J.R.S., Levine, S.E., Corsetti, J.R., Reilly, T., Landsman, A.S., Williams, J.L., Thibault, L.E., 1996. The biochemical pathway mediating the proliferative response of bone cells to a mechanical stimulus. *Journal of Bone and Joint Surgery* **78 (A)**, 1337-1347.

[5] Yousefan, J., Firouzian, F., Shanfeld, J.,Ngan, P., Lanese, R.,Davidovitch, Z., 1995. A new experimental model for studying the response of periodontal ligament cells to hydrostatic pressure. *American Journal of Orthodontics and Dentofacial Orthopaedics* **108**, 402-409.

[6] Guldberg RE, Caldwell NJ, Guo XE, Goulet RW, Hollister SJ, Goldstein SA. Mechanical stimulation of tissue repair in the hydraulic bone chamber. *J Bone Miner Res* 1997; **12(8)**: 1295-1302.

[7] Torzilli, P.A., Grigiene, R., Huang, C., Friedman, S.M., Doty, S.B., Boskey, A.L., Lust, G., 1997. Characterization of cartilage metabolic response to static and dynamic stress using a mechanical explant test system. *Journal of Biomechanics* **30**, 1-9.

[8] Freeman, P.M., Natarajan, R.N., Kimura, J.H., Andriacchi, T.P., 1994. Chondrocyte cells respond mechanically to compressive loads. *Journal of Orthopaedic Research* **12,** 311-320.

[9] Cheng, G.C., Libby, P., Grodzinsky, A.J., Lee, R.T., 1996. Induction of DNA synthesis by a single transient mechanical stimulus of human vascular smooth muscle cells. *Role of "broblast growth factor-2. Circulation* **93**, 99 -105.

[10] Brown TD. Techniques for mechanical stimulation of cells in vitro: a review. *Journal of Biomechanics* 2000; **33**: 3-14.

[11] Dewitt, M.T., Handley, C.J., Oakes, B.W., Lowther, D.A., 1984. In vitro response of chondrocytes to mechanical loading. The effects of short term mechanical tension. *Connective Tissue Research* **12**, 97 -109.

[12] Murray, D.W., Rushton, N., 1990. The effect of strain on bone cell prostaglandin E2 release: a new experimental method. *Calcified Tissue International* **47**, 35-39.

[13] Mitton, M.P., Tumminia, S.J., Arora, J., Zelenka, P., Epstein, D.L., Russell, P., 1997. Transient loss of alphaB-crystallin: an early cellular response to mechanical stretch. *Biochemistry and Biophysical Research Communication* **235**, 69 -73.

[14] Bynum, D.K., Tsuzaki, M., Yang, X., Sood, A., Brown, T.D., Ross, A., Weinhold, P., Banes, A.J., 1999. Inhibiting intercellular communication blocks wound-induced mitogenesis in flexor tendons. *Transaction of 45th Annual Meeting Orthopaedic Research Society*, p. 44.

[15] Banes, A.J., Gilbert, J.L., Taylor, T., Monbureau, O., 1985. A new vacuum-operated stress-providing instrument that applies static or variable duration cyclic tension or compression to cells in vitro. *Journal of Cell Science* **75**, 35-42.

[16] Brown, T.D., Pedersen, D.R., Bottlang, M., Banes, A.J., 1997. Fluid-structure interaction as a determinant of nutrient medium reactive stress in mechanically stimulated cultures. *Transaction of 43rd Annual Meeting Orthopaedic Research Society*, p. 175.

[17]Lai, Y., MacDonald, J., Hubbard, T. and Kujath, M., "Force, Deflection and Power Measurements of Toggled Micro Thermal Motors", *J of Micromech. and MicroEng.*, **14(1)**, 2004, pp.49-56.

[18]Lai, Y., Bordatchev, E.V., Nikumb, S.K., Hsu, W., "Performance Characterization of In-plane Electro-Thermally Driven Linear Microactuators", *J. of Intelligent Material Systems and Structures,* 2006, 17 (10), pp. 919-929.

[19]Lai, Y., Kujath, M., and Hubbard, T., "Modal Simulation and Testing of a Micro-manipulator", *ASME Trans. J of Dynam. Syst., Meas. and Control*, **127(3)**, 2005, pp.515-519.

[20]Lai, Y., Belisle, A., Kujath, M. and Hubbard, T., "Micromachined Planar Grippers", *IFToMM 11th World Congress in Mechanism and Machine Science*, 2004, pp.1432-1437, Tianjin, China.

[21] Lai, Y., Kujath, M., and Hubbard, T., "Motion Control of a Compliant Micro Manipulator", *7th IFAC Symposium on Robot Control (SYROCO)*, September 2003, Wroclaw, Poland.

[22]Lai, Y., Bordacthev, E. and Nikumb, S., "Metallic capacitive sensor by laser fabrication technology", *Journal of Microsystem Technologies*, 2006, 12(8), pp.778-785.

[23] Erdman, A.G. and Sandor, G.N., *Mechanism Design-Analysis and Synthesis*, 1997, 3rd Ed., Chapter 1, Page 24, Prentice Hall, Upper Saddle River, New Jersey.